INTERNATIONAL JOURNAL FOR NUMERICAL AND ANALYTICAL METHODS IN GEOMECHANICS, VOL. 21, 15–42 (1997)

NON-LINEAR WAVE-INDUCED RESPONSE OF POROUS SEABED: A FINITE ELEMENT ANALYSIS

D. S. JENG*

Department of Environmental Engineering, The University of Western Australia, Nedlands, WA 6907, Australia

AND

Y. S. LIN

Department of Civil Engineering, National Chung-Hsing University, Taichung 40227, Taiwan, R.O.C.

SUMMARY

Conventional investigations of waves–seabed interaction problems have been only concerned with the soil response due to two-dimensional linear progressive waves over a *uniform* seabed. However, the effects of non-linear waves which have been reported in the literature may be significantly different. In this paper, a finite element model is developed to investigate the non-linear wave-induced seabed response with variable permeability and shear modulus in a three-dimensional domain. The finite element formulations are fully presented in this paper. The numerical model is verified with the previous investigations through the reduced form of the present solution. The numerical results indicate that the influence of non-linear wave components cannot always be ignored without substantial error. Furthermore, the wave-induced seabed response is affected significantly by variable permeability in coarser seabeds and variable shear modulus in finer seabeds.

KEY WORDS: variable permeability and shear modulus; non-linear wave; finite element model

1. INTRODUCTION

A detailed knowledge of wave-induced variation in pore pressure and effective stresses in a porous seabed plays an important role in analysing seabed stability and its effects on marine structures. It has been well documented in the literature that waves propagating over the ocean can create significant dynamic pressure fluctuations on sea floors. This pressure fluctuation induces a stress field and excess pore water pressure in marine sediments, which may be significant enough to cause shear failure and liquefaction in the sediments, leading to seabed instability.[1]

Generally speaking, two mechanisms of wave-induced soil response have been observed in laboratory experiments and field measurements.[2,3] The first mechanism is characterized by the generation of residual pore pressure due to cyclic shearing of the soil. This type of soil response appears in the initial stage of cyclic loading. It is similar to that induced by earthquakes, which results in the build-up of excess pore pressure. The second mechanism occurs due to transient changes in mean effective stresses, accompanied by the damping of amplitudes and phase lags in the pore pressure. In this study, only transient soil response will be considered.

* Corresponding author

CCC 0363–9061/97/010015–28

Received 25 January 1996
Revised 30 May 1996

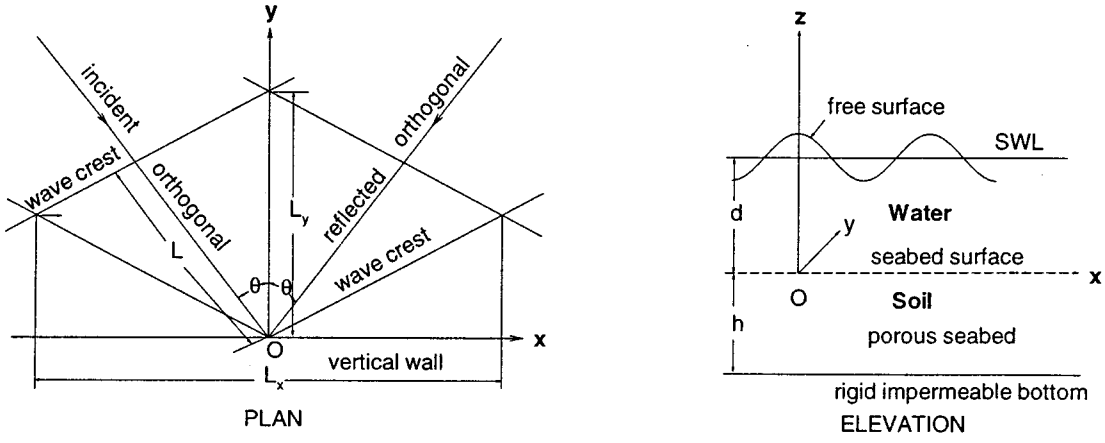

Figure 1. Definition sketch of short-crested wave system produced by oblique reflection from a breakwater

Numerous uncoupled analyses have considered various conditions such as a rigid and non-deformable porous medium with an isotropic permeability and incompressible pore fluid,[4,5] hydraulically anisotropic permeability,[6] stratified permeability,[7] and with compressible pore fluid.[8] Since these theories assume that the seabed is a rigid porous medium, they do not include the coupling of pore fluid motion and soil deformation. The governing equation becomes Laplace's equation for incompressible fluid, and the diffusion equation for a compressible pore fluid. Therefore, such solutions for pore pressure are limited to particular ideal cases of soil and wave conditions. Furthermore, these approaches provide no information on soil stresses which is essential, when elastic waves in soils are considered.

Based on Biot's consolidation theory[9] and the storage equation,[10] a more realistic approach has considered a compressible pore fluid in a compressible porous medium,[11–16] and in a cross-anisotropic seabed.[17,18] Various numerical solutions have also been obtained by using finite difference methods[19,20] or finite element methods[21,22] and boundary element methods.[23] However, the above approaches are only related to two-dimensional linear progressive and standing waves.

In general, breakwaters and seawalls are often oriented obliquely to the direction of predominant swell and storm waves, resulting in the formulation of a short-crested wave system in front of such structures. The isolated crests form at the intersections of the incident and reflected waves (Figure 1). The resulting water surface undulation has double periodicity, and is characterized by a pattern of island crests formed at the intersections of the incident and reflected waves. This provides not only a new wavelength (L_x), but also a definitive wave crest length (L_y), which is the distance between two simultaneous crests normal to the wall. These waves are hence referred to as 'short-crested'.

The short-crested wave system has attracted great attention from coastal engineers in recent years, because it produces a larger wave force and energy than two-dimensional progressive and standing waves.[24–26] In general, most investigations of the short-crested wave system have only examined its kinematic and dynamic properties, rather than on the wave-induced seabed response. However, an interest in the latter has been developed due to the possibility that some marine structures have failed because of liquefaction within the seabed.[27–29]

Recently, a series of studies for the short-crested wave-induced soil response in an elastic seabed have been systematically developed.[30–37] Among these, the authors have only concerned with the

soil response due to linear waves, ignoring the effect of non-linearity. However, the effects of non-linear wave components cannot always be neglected without substantial error, especially for large waves in shallow water.[38–40] Thus, it is useful to examine the effect of non-linear waves on the seabed response under such conditions.

The permeability of a porous seabed is a measure of how rapidly fluid is transmitted through the voids between grains. Marine sediments below the water–soil interface undergo consolidation due to both the overburden soil pressure and the water pressure above it. This results in a decrease in void ratio and porosity, accompained by an increase in the unit weight of the soil. An example of permeability varying with burial depth (z) was reported for marine sediments in the Gulf of Mexico.[41] Similar evidence for soil consolidation versus depth can also be found in the literature.[42]

The shear modulus of soil is defined as the proportional constant in the shear stress–shear strain relation. For the consolidation problem, the medium whose shear modulus increases linearly with depth (so called *Gibson Soil*) has been studied,[43] but without water wave loading. Most theoretical approaches for water–soil interaction in the literature have assumed the soil shear modulus as uniform throughout the soil matrix. However, in nature, the rigidity of the soil generally increases with depth as a consequence of the increasing effective overburden pressure. There are really volumes of evidences that this occurs depending on the geology.[44]

The major difficulty in understanding the wave–seabed interaction phenomenon for a porous seabed with variable permeability and shear modulus has been the complexity in the mathematical expressions of the dynamic behaviour of the soil and pore fluid. Thus, only a few investigations have attempted to treat this problem within a multiply layered medium.[7,13,22,32,33] However, these theories are valid only for *uniform* soil characteristics in each sublayer. Therefore, the horizontal normal stresses and gradients of all stress components discontinue at the interface between sublayers. Since the seabed responses should vary continuously with burial depth in a natural seabed, these discontinuities may cause inaccuracy in evaluating the wave-induced seabed response. This may lead to substantial errors in stability analyses of foundations.

The aims of this study are to investigate the influences of (1) the non-linearity of water waves and (2) variable permeability and shear modulus on the wave-induced soild response in front of a marine structure. Firstly, the finite element formulation of the resulting equations is derived. The verification of the numerical model against the previous experimental data is then presented. Based on the present model, the effects of non-linear wave components, variable permeability and shear modulus on the seabed response will be discussed in detail.

2. BOUNDARY VALUE PROBLEM

In this study, we consider a soil column of finite thickness h in a sedimentary seabed fronting a vertical reflecting wall, as depicted in Figure 1. A short-crested wave system is produced by full oblique reflection of the incident waves, with obliquity angle θ measured between a wave orthogonal and the normal direction to the wall,[45] and also between the wave crests and the wall itself. The resultant wave crests are assumed to propagate in the positive x-axis parallel to the wall. The y-axis is normal to it, while the z-axis is upward from the water–soil interface (termed as the *seabed surface*).

Based on the Biot's 3-D consolidation theory,[9] with the storage equation,[10] the governing equation for the wave–soil interaction problem within a compressible pore fluid in a compressible porous seabed with variable permeability is

$$\frac{k_x}{k_z}\frac{\partial^2 p}{\partial x^2}+\frac{k_y}{k_z}\frac{\partial^2 p}{\partial y^2}+\frac{\partial^2 p}{\partial z^2}+\frac{1}{k_z}\frac{\mathrm{d}k_z}{\mathrm{d}z}\frac{\partial p}{\partial z}-\frac{\gamma_w n'\beta}{k_z}\frac{\partial p}{\partial t}=\frac{\gamma_w}{k_z}\frac{\partial \varepsilon}{\partial t} \tag{1}$$

It is worth noting that the fourth term on the left-hand side of equation (1) comes from variable permeability, which vanishes for a *uniform* seabed.

In equation (1), k_x, k_y and k_z are the components of soil hydraulic permeability in the x-, y- and z-directions, respectively; p is the wave-induced pore pressure; γ_w is the unit weight of the pore water; n' is soil porosity; β is the compressibility of the pore fluid; t is time and ε is the volume strain defined by

$$\varepsilon = \frac{\partial u}{\partial x} + \frac{\partial v}{\partial y} + \frac{\partial w}{\partial z} \tag{2}$$

in which u, v and w are the soil displacements in the x-, y- and z-directions, respectively. The compressibility of the pore fluid β can be related to the apparent bulk modulus of the pore water K' and the degree of saturation S_r, such that

$$\beta = \frac{1}{K'} = \frac{1}{K_w} + \frac{1 - S_r}{P_{w0}} \tag{3}$$

where K_w is the true bulk modulus of elasticity of water, and P_{w0} is the absolute pore-water pressure. If the soil skeleton is absolutely air-free, i.e. fully saturated, then $K' = K_w$, since $S_r = 1$.

Based on the effective stress concept, the three-dimensional force equilibrium in the absence of body forces within the soil skeleton can be written as

$$\frac{\partial \sigma'_x}{\partial x} + \frac{\partial \tau'_{xy}}{\partial y} + \frac{\partial \tau'_{xz}}{\partial z} = \frac{\partial p}{\partial x} \tag{4}$$

$$\frac{\partial \tau'_{xy}}{\partial x} + \frac{\partial \sigma'_y}{\partial y} + \frac{\partial \tau'_{yz}}{\partial z} = \frac{\partial p}{\partial y} \tag{5}$$

and

$$\frac{\partial \tau'_{xz}}{\partial x} + \frac{\partial \tau'_{yz}}{\partial y} + \frac{\partial \sigma'_z}{\partial z} = \frac{\partial p}{\partial z} \tag{6}$$

in the x-, y- and z-directions, respectively.

Herein, the soil skeleton generally obeys Hooke's law, implying linear, reversible and non-retarded mechanical properties. Thus, the relationship between effective stresses and soil displacements may be expressed as

$$\sigma'_x = 2G(z)\left[\frac{\partial u}{\partial x} + \frac{\mu}{1 - 2\mu}\varepsilon\right] \tag{7}$$

$$\sigma'_y = 2G(z)\left[\frac{\partial v}{\partial y} + \frac{\mu}{1 - 2\mu}\varepsilon\right] \tag{8}$$

$$\sigma'_z = 2G(z)\left[\frac{\partial w}{\partial z} + \frac{\mu}{1 - 2\mu}\varepsilon\right] \tag{9}$$

$$\tau'_{xy} = G(z)\left[\frac{\partial u}{\partial y} + \frac{\partial v}{\partial x}\right] = \tau'_{yx} \tag{10}$$

$$\tau'_{xz} = G(z)\left[\frac{\partial u}{\partial z} + \frac{\partial w}{\partial x}\right] = \tau'_{zx} \tag{11}$$

$$\tau'_{yz} = G(z)\left[\frac{\partial v}{\partial z} + \frac{\partial w}{\partial y}\right] = \tau'_{zy} \tag{12}$$

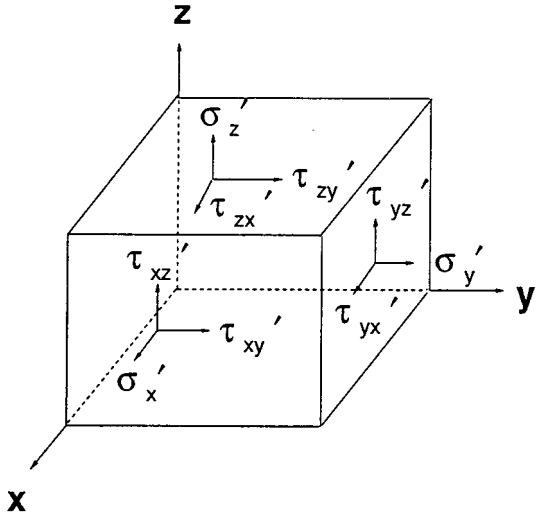

Figure 2. Definition sketch of a stress block on a soil element in the domain of soil skeleton

where the Cauchy stress tensor on the adjacent faces of stress element consists of three effective normal stresses and six shear stress components. The shear stresses are expressed in double subscripts denoting the stress in the s-direction on a plane perpendicular to the r-axis (Figure 2). The shear modulus of the soil $G(z)$ is related to the Young's modulus $E(z)$ by the Poisson's ratio μ, according to $G = E/(1 + 2\mu)$.

Substituting the stress–strain relationship, equations (7)–(12), into equations (4)–(6), the equations of force equilibrium within the soil matrix can be rewritten as

$$G(z)\nabla^2 u + \frac{G(z)}{(1-2\mu)}\frac{\partial \varepsilon}{\partial x} + \frac{\mathrm{d}G(z)}{\mathrm{d}z}\left[\frac{\partial u}{\partial z} + \frac{\partial w}{\partial x}\right] = \frac{\partial p}{\partial x} \tag{13}$$

$$G(z)\nabla^2 v + \frac{G(z)}{(1-2\mu)}\frac{\partial \varepsilon}{\partial y} + \frac{\mathrm{d}G(z)}{\mathrm{d}z}\left[\frac{\partial v}{\partial z} + \frac{\partial w}{\partial y}\right] = \frac{\partial p}{\partial y} \tag{14}$$

and

$$G(z)\nabla^2 w + \frac{G(z)}{(1-2\mu)}\frac{\partial \varepsilon}{\partial z} + \frac{\mathrm{d}G(z)}{\mathrm{d}z}\left[\frac{2\mu}{1-2\mu}\left(\frac{\partial u}{\partial x} + \frac{\partial v}{\partial y}\right) + \frac{2(1-\mu)}{1-2\mu}\frac{\partial w}{\partial z}\right] = \frac{\partial p}{\partial z} \tag{15}$$

in the x-, y- and z-directions, respectively.

The governing equations (1) and (13)–(15), describing the water–soil interaction problem, can be solved incorporating the boundary conditions specified at the seabed surface and the impermeable bottom, respectively.

For a soil matrix, the mathematical expression for the wave-induced soil response can be derived subject to some appropriate boundary conditions. Firstly, for the soil resting on an impermeable rigid base underneath a finite thickness, zero displacements and no vertical flow occurs (Figure 1),

$$u = v = w = \frac{\partial p}{\partial z} = 0 \quad \text{at } z = -h \tag{16}$$

Secondly, the vertical effective normal stress and shear stresses vanish at the seabed surface. The pore pressure on this upper soil boundary is given by the wave pressure at the seabed:

$$\sigma'_z = \tau'_{xz} = \tau'_{yz} = 0, \qquad p = P_b \quad \text{at } z = 0 \tag{17}$$

in which P_b is the wave pressure at the seabed surface. The general form of P_b for the Nth-order short-crested wave theory can be expressed as[45]

$$P_b = p_0 \sum_{r=0}^{N} \sum_{s=1}^{N-r} C_{rs} \cos sn\lambda y \cos r(m\lambda x - \omega t) \quad \text{at } z = 0 \tag{18}$$

where $\cos sn\lambda y \cos r(m\lambda x - \omega t)$ denotes the spatial and temporal variations in a 3-D wave field, such as the short-crested wave described in this study.

It has been agreed that the wave profile has steep crest and flat trough in shallow water, resulted from its strong non-linearity. Therefore, the validity of the conventional Stokes' wave theories in shallow water has been doubted. As Huang *et al.*[40] and Sobey *et al.*[46] pointed out, Stokes' wave theories may not be very good model for a wave in shallow water near the breaking line. However, it is acceptable under most wave conditions for engineering application. In fact, engineering practice in recent decades has still replied heavily on the Stokes' theory because it performs the basic characteristics of wave non-linearity and its accuracy satisfies requirements of most engineering problems. Since the investigation of wave non-linearity on the soil response have not been available until now, we consider the second-order wave theory to achieve this aim at this beginning stage of this study.

In equation (18), the coefficients C_{rs} for the second-order solution are[45]

$$C_{11} = 1 \tag{19}$$

$$C_{02} = -\frac{\lambda H_s}{16 \sinh \lambda d}(2m^2 - 1)(1 - \omega_0^4) \tag{20}$$

$$C_{20} = \frac{\lambda H_s}{16 \sinh \lambda d}\left\{(1 - 2m^2)(1 - \omega_0^4) + \frac{(1 + \omega_m^4)(4m^2 - 1 - 3\omega_0^4)}{(1 + \omega_m^4 - m\omega_m^2/\omega_0^2)\cosh 2m\lambda d}\right\} \tag{21}$$

$$C_{22} = \frac{\lambda H_s}{16 \sinh \lambda d}\left\{-(1 - \omega_0^4) + \frac{3(\omega_0^{-4} - \omega_0^4)}{\cosh 2\lambda d}\right\} \tag{22}$$

$$\omega_0^2 = g\lambda \tanh \lambda d \quad \text{and} \quad \omega_m^2 = g\lambda \tanh m\lambda d \tag{23}$$

The amplitude factor p_0 in equation (18) is related to the wave pressure of the first order of the short-crested wave theory,

$$p_0 = \frac{\gamma_w H_s}{2 \cosh \lambda d} \tag{24}$$

where H_s is the wave height of the short-crested waves; λ is the wave number of the incident and the reflected waves ($\lambda = 2\pi/L$, in which L is the wave length); ω is the angular frequency of the wave ($\omega = 2\pi/T$, T is the wave period); and d is the water depth above the seabed surface.

Parameters m and n are the obliquity components relating to the wave number λ in the x- and y-directions, respectively,

$$\lambda_x = 2\pi/L_x = m\lambda = \lambda \sin\theta \quad \text{and} \quad \lambda_y = 2\pi/L_y = n\lambda = \lambda \cos\theta \tag{25}$$

where L_x and L_y are the wavelength and crest length of the short-crested waves (Figure 1). From equation (25), the relationship $m^2 + n^2 = 1$ is applicable to the short-crested wave system.

3. FINITE ELEMENT FORMULATION

The governing equations (1) and (13)–(15) for wave-induced soil response in a porous seabed can be solved by combining semi-analytical techniques with a finite element Galerkin method.[47] The three-dimensional boundary value problem can be reduced to one-dimensional form by assuming simple harmonic pressure wave loading on the surface of the seabed.

Employing the principle of superposition to incorporate the solution produced for the incident and reflected wave components (Figure 1), the wave-induced pore pressure, soil displacements and effective stresses are assumed in a general form for the first-order solution as

$$f(x, y, z) = f_a(z)e^{i(m\lambda x + n\lambda y - \omega t)} + f_b(z)e^{i(m\lambda x - n\lambda y - \omega t)} \tag{26}$$

$$f = \{p, u, v, w, \sigma'_x, \sigma'_y, \sigma'_z, \tau'_{xy}, \tau'_{xz}, \tau'_{yz}\}^T \tag{27}$$

$$f_a = \{p_a, u_a, v_a, w_a, \sigma'_{xa}, \sigma'_{ya}, \sigma'_{za}, \tau'_{xya}, \tau'_{xza}, \tau'_{yza}\}^T \tag{28}$$

$$f_b = \{p_b, u_b, v_b, w_b, \sigma'_{xb}, \sigma'_{yb}, \sigma'_{zb}, \tau'_{xyb}, \tau'_{xzb}, \tau'_{yzb}\}^T \tag{29}$$

The first term on the right-hand side of equation (26) represents the contribution from the reflected waves, while the second term is for the incident waves. The solutions for the wave-induced soil response can be found separately and then superimposed to yield the complete solution required. Following the same procedure, the seabed response due to the second-order wave components can also be obtained.

For convenience, the function f_a can be further separated into real and imaginary parts as

$$f_a(z) = f_r + if_c \tag{30}$$

$$f_r = \{P_r, U_r, V_r, W_r, S_{xr}, S_{yr}, S_{zr}, T_{xyr}, T_{xzr}, T_{yzr}\}^T \tag{31}$$

$$f_c = \{P_c, U_c, V_c, W_c, S_{xc}, S_{yc}, S_{zc}, T_{xyc}, T_{xzc}, T_{yzc}\}^T \tag{32}$$

in which f_r and f_c denote the real and imaginary parts of f_a, respectively. In equations (31) and (32), $P, U, V, W, S_x, S_y, S_z, T_{xy}, T_{xz}$ and T_{yz} are related to $p, u, v, w, \sigma'_x, \sigma'_y, \sigma'_z, \tau'_{xy}, \tau'_{xz}$, and τ'_{yz} respectively.

Substituting equation (30) into the governing equation (1), and then directly applying the Galerkin method[46] to these equations, the finite element analytical formulations can be obtained as

$$\begin{aligned} N_i \begin{Bmatrix} dP_r/dz \\ dP_c/dz \end{Bmatrix}_0^{L_e} = {} & \int_0^{L_e} \frac{dN_i}{dz} \begin{Bmatrix} dP_r/dz \\ dP_c/dz \end{Bmatrix} dz + \int_0^{L_e} N_i \lambda^2 \left(\frac{m^2 k_x + n^2 k_y}{k_z} \right) \begin{Bmatrix} P_r \\ P_c \end{Bmatrix} dz \\ & + \int_0^{L_e} N_i \frac{\gamma_w n' \beta \omega}{k_z} \begin{Bmatrix} P_c \\ -P_r \end{Bmatrix} dz + \int_0^{L_e} N_i \frac{m\lambda\gamma_w \omega}{k_z} \begin{Bmatrix} U_r \\ U_c \end{Bmatrix} dz \\ & + \int_0^{L_e} N_i \frac{n\lambda\gamma_w \omega}{k_z} \begin{Bmatrix} V_r \\ V_c \end{Bmatrix} dz + \int_0^{L_e} N_i \frac{\gamma_w \omega}{k_z} \begin{Bmatrix} dW_c/dz \\ dW_r/dz \end{Bmatrix} dz \\ & - \int_0^{L_e} N_i \frac{1}{k_z} \frac{dk_z}{dz} \begin{Bmatrix} dP_r/dz \\ dP_c/dz \end{Bmatrix} dz \end{aligned} \tag{33}$$

in which L_e is the length of element, while N_i represents the shape function of ith node ($i = 1, 2, \ldots, n_e$) and n_e is the number of nodes per element.

Introducing equation (30) into equation (13), the finite element form is given as

$$\int_0^{L_e} N_i m\lambda \begin{Bmatrix} P_c \\ -P_r \end{Bmatrix} dz - \int_0^{L_e} N_i G \left(\lambda^2 + \frac{m^2\lambda^2}{1-2\mu}\right) \begin{Bmatrix} U_r \\ U_c \end{Bmatrix} dz - \int_0^{L_e} N_i \frac{mnG\lambda^2}{1-2\mu} \begin{Bmatrix} V_r \\ V_c \end{Bmatrix} dz$$
$$+ \int_0^{L_e} N_i G \begin{Bmatrix} dW_c/dz \\ -dW_r/dz \end{Bmatrix} dz + \int_0^{L_e} N_i G \begin{Bmatrix} d^2U_r/dz^2 \\ d^2U_c/dz^2 \end{Bmatrix} dz + \int_0^{L_e} N_i \frac{dG}{dz} \begin{Bmatrix} dU_r/dz \\ dU_c/dz \end{Bmatrix} dz$$
$$+ \int_0^{L_e} N_i im\lambda \frac{dG}{dz} \begin{Bmatrix} -W_c \\ W_r \end{Bmatrix} dz = 0 \tag{34}$$

Applying the principle of partial integration to the first and fourth terms in the above equation renders to

$$N_i \begin{Bmatrix} T_{xzr} \\ T_{xzc} \end{Bmatrix}_0^{L_e} = \int_0^{L_e} N_i G \left(\lambda^2 + \frac{m^2\lambda^2}{1-2\mu}\right) \begin{Bmatrix} U_r \\ U_c \end{Bmatrix} dz + \int_0^{L_e} N_i \frac{mnG\lambda^2}{1-2\mu} \begin{Bmatrix} V_r \\ V_c \end{Bmatrix} dz$$
$$+ \int_0^{L_e} N_i \frac{2mG\lambda\mu}{1-2\mu} \begin{Bmatrix} dW_c/dz \\ -dW_r/dz \end{Bmatrix} dz + \int_0^{L_e} \frac{dN_i}{dz} G \begin{Bmatrix} dU_r/dz \\ dU_c/dz \end{Bmatrix} dz$$
$$+ \int_0^{L_e} \frac{dN_i}{dz} Gm\lambda \begin{Bmatrix} -W_c \\ W_r \end{Bmatrix} dz + \int_0^{L_e} N_i m\lambda \begin{Bmatrix} -P_c \\ P_r \end{Bmatrix} dz \tag{35}$$

Similarly, equations (14) and (15) can also be derived in finite element form as

$$N_i \begin{Bmatrix} T_{yzr} \\ T_{yzc} \end{Bmatrix}_0^{L_e} = \int_0^{L_e} N_i G \left(\lambda^2 + \frac{n^2\lambda^2}{1-2\mu}\right) \begin{Bmatrix} V_r \\ V_c \end{Bmatrix} dz + \int_0^{L_e} N_i \frac{mnG\lambda^2}{1-2\mu} \begin{Bmatrix} U_r \\ U_c \end{Bmatrix} dz$$
$$+ \int_0^{L_e} N_i \frac{2nG\lambda\mu}{1-2\mu} \begin{Bmatrix} dW_c/dz \\ -dW_r/dz \end{Bmatrix} dz + \int_0^{L_e} \frac{dN_i}{dz} G \begin{Bmatrix} dV_r/dz \\ dV_c/dz \end{Bmatrix} dz$$
$$+ \int_0^{L_e} \frac{dN_i}{dz} Gn\lambda \begin{Bmatrix} -W_c \\ W_r \end{Bmatrix} dz + \int_0^{L_e} N_i n\lambda \begin{Bmatrix} -P_c \\ P_r \end{Bmatrix} dz \tag{36}$$

and

$$N_i \begin{Bmatrix} S_{zr} \\ S_{zc} \end{Bmatrix}_0^{L_e} = \int_0^{L_e} \frac{dN_i}{dz} G \frac{2(1-\mu)}{1-2\mu} \begin{Bmatrix} dW_r/dz \\ dW_c/dz \end{Bmatrix} dz + \int_0^{L_e} N_i G\lambda^2 \begin{Bmatrix} W_r \\ W_c \end{Bmatrix} dz$$
$$+ \int_0^{L_e} N_i mG\lambda \begin{Bmatrix} dU_c/dz \\ -dU_r/dz \end{Bmatrix} dz + \int_0^{L_e} \frac{dN_i}{dz} \frac{2mG\lambda\mu}{1-2\mu} \begin{Bmatrix} -U_c \\ U_r \end{Bmatrix} dz$$
$$+ \int_0^{L_e} \frac{dN_i}{dz} \frac{2nG\lambda\mu}{1-2\mu} \begin{Bmatrix} -V_c \\ V_r \end{Bmatrix} dz + \int_0^{L_e} N_i Gn\lambda \begin{Bmatrix} dV_c/dz \\ -dV_r/dz \end{Bmatrix} dz$$
$$+ \int_0^{L_e} N_i \begin{Bmatrix} dP_r/dz \\ dP_c/dz \end{Bmatrix} dz \tag{37}$$

In the above equations, eight variables, P_r, P_c, U_r, U_c, V_r, V_c, W_r and W_c can be expressed by the shape function and nodal values of the variables in matrix form as

$$\{\mathbf{q}\} = [\mathbf{N}]\{\mathbf{q}_e\} \tag{38}$$

$$\{\mathbf{q}\}^T = \{P_r, P_c, U_r, U_c, V_r, V_c, W_r, W_c\} \tag{39}$$

$$\{\mathbf{q}_e\}^T = \{q_i^T, \ldots, q_{n_e}^T\} \tag{40}$$

$$\{q_j\}^T = \{P_{rj}, P_{cj}, U_{rj}, U_{cj}, V_{rj}, V_{cj}, W_{rj}, W_{cj}\}, \quad j = 1, 2, \ldots, n_e \tag{41}$$

$$[\mathbf{N}] = [N_1\mathbf{I}, N_2\mathbf{I}, \ldots, N_{n_e}\mathbf{I}] \tag{42}$$

Introducing equation (38) into equations (33) and (35)–(37), it can be expressed in matrix form as

$$\{\mathbf{F}_e\} = \left[\int_0^{L_e} \mathbf{B}_1^T\mathbf{D}_1\mathbf{B}_1\,\mathrm{d}z + \int_0^{L_e} \mathbf{B}_1^T\mathbf{D}_2\mathbf{B}_2\,\mathrm{d}z + \int_0^{L_e} \mathbf{B}_2^T\mathbf{D}_3\mathbf{B}_1\,\mathrm{d}z + \int_0^{L_e} \mathbf{B}_2^T\mathbf{D}_4\mathbf{B}_2\,\mathrm{d}z\right]\{\mathbf{q}_e\},$$

$$= [\mathbf{K}_e]\{\mathbf{q}_e\} \tag{43}$$

$$\{\mathbf{F}_e\}^T = \left\{-\left(\frac{\mathrm{d}P_r}{\mathrm{d}z}\right)_1,\ -\left(\frac{\mathrm{d}P_c}{\mathrm{d}z}\right)_1,\ -(T_{xzr})_1,\ -(T_{xzc})_1,\ -(T_{yzr})_1,\ -(T_{yzc})_1,\right.$$

$$-(S_{zr})_1,\ -(S_{zc})_1, \underbrace{0, 0, 0, \ldots, 0, 0}_{8\times(n_e-2)}, \left(\frac{\mathrm{d}P_r}{\mathrm{d}z}\right)_{n_e}, \left(\frac{\mathrm{d}P_c}{dz}\right)_{n_e},$$

$$\left.(T_{xzr})_{n_e}, (T_{xzc})_{n_e}, (T_{yzr})_{n_e}, (T_{yzc})_{n_e}, (S_{zr})_{n_e}, (S_{zc})_{n_e}\right\} \tag{44}$$

$$\mathbf{B}_1 = [B_{11}, B_{12}, B_{13}, \ldots, B_{1n_e}], \quad B_{1i} = N_i\mathbf{I}, \tag{45}$$

$$\mathbf{B}_2 = [B_{21}, B_{22}, B_{23}, \ldots, B_{2n_e}], \quad B_{2i} = \frac{\mathrm{d}N_i}{\mathrm{d}z}\mathbf{I} \tag{46}$$

in which $\mathbf{I}$ is an 8×8 identity matrix, $\mathbf{D}_i$ ($i = 1, 2, 3, 4$) is an 8×8 matrix (Appendix I).

The individual element equation (43) must be assembled appropriately to obtain the global equation as follows:

$$\{\mathbf{F}\} = [\mathbf{K}]\{\mathbf{q}\} \tag{47}$$

$$\{\mathbf{F}_e\}^T = \left\{-\left(\frac{\mathrm{d}P_r}{\mathrm{d}z}\right)_1,\ -\left(\frac{\mathrm{d}P_c}{\mathrm{d}z}\right)_1,\ -(T_{xzr})_1,\ -(T_{xzc})_1,\ -(T_{yzr})_1,\ -(T_{yzc})_1,\right.$$

$$-(S_{zr})_1,\ -(S_{zc})_1, \underbrace{0, 0, 0, \ldots, 0, 0}_{8\times(N_p-2)}, \left(\frac{\mathrm{d}P_r}{\mathrm{d}z}\right)_{N_p}, \left(\frac{\mathrm{d}P_c}{\mathrm{d}z}\right)_{N_p},$$

$$\left.\times(T_{xzr})_{N_p}, (T_{xzc})_{N_p}, (T_{yzr})_{N_p}, (T_{yzc})_{N_p}, (S_{zr})_{N_p}, (S_{zc})_{N_p}\right\} \tag{48}$$

in which N_p is the total number of nodal points. Employing the boundary conditions, equations (16)–(18), the global equation (47) can be solved. The wave-induced pore pressure and soil displacements can then be obtained.

In the conventional finite element method, the stresses are calculated from the nodal displacements by Hooke's law. However, this iteration may cause inaccuracy in calculating the stress values at the nodes. To avoid this numerical inaccuracy, we derive directly the finite element formulation from the equations of force equilibrium, (13)–(15). Three effective stresses T_{xz}, T_{yz} and S_z have been derived as equations (35)–(37). Similarly, the other three effective stresses S_x, S_y and T_{xy} can also be derived as follows.

Substituting equation (30) into equations (13)–(15), after some algebraic manipulation, renders the final form as

$$
\begin{aligned}
N_i \begin{Bmatrix} S_{xr} \\ S_{xc} \end{Bmatrix}_0^{L_e} = {} & \int_0^{L_e} \frac{dN_i}{dz} \frac{2G\mu}{1-2\mu} \begin{Bmatrix} dW_r/dz \\ dW_c/dz \end{Bmatrix} dz + \int_0^{L_e} \frac{dN_i}{dz} \frac{2mG\lambda(1-\mu)}{1-2\mu} \begin{Bmatrix} -U_c \\ U_r \end{Bmatrix} dz \\
& + \int_0^{L_e} \frac{dN_i}{dz} \frac{2nG\lambda\mu}{1-2\mu} \begin{Bmatrix} -V_c \\ V_r \end{Bmatrix} dz + \int_0^{L_e} N_i \frac{G\lambda^2\mu}{1-\mu} \begin{Bmatrix} W_r \\ W_c \end{Bmatrix} dz \\
& + \int_0^{L_e} N_i \frac{mG\lambda(2-\mu)}{(1-\mu)} \begin{Bmatrix} -dU_c/dz \\ dU_r/dz \end{Bmatrix} dz + \int_0^{L_e} N_i \frac{nG\lambda\mu}{1-\mu} \begin{Bmatrix} -dV_c/dz \\ dV_r/dz \end{Bmatrix} dz \\
& + \int_0^{L_e} N_i \frac{dG}{dz} \frac{m\lambda}{(1-\mu)} \begin{Bmatrix} -U_c \\ U_r \end{Bmatrix} dz + \int_0^{L_e} N_i \frac{dG}{dz} \frac{n\lambda\mu}{1-\mu} \begin{Bmatrix} -V_c \\ V_r \end{Bmatrix} dz \\
& + \int_0^{L_e} N_i \frac{\mu}{(1-\mu)} \begin{Bmatrix} dP_r/dz \\ dP_c/dz \end{Bmatrix} dz
\end{aligned} \tag{49}
$$

$$
\begin{aligned}
N_i \begin{Bmatrix} S_{yr} \\ S_{yc} \end{Bmatrix}_0^{L_e} = {} & \int_0^{L_e} \frac{dN_i}{dz} \frac{2G\mu}{1-2\mu} \begin{Bmatrix} dW_r/dz \\ dW_c/dz \end{Bmatrix} dz + \int_0^{L_e} \frac{dN_i}{dz} \frac{2nG\lambda(1-\mu)}{1-2\mu} \begin{Bmatrix} -V_c \\ V_r \end{Bmatrix} dz \\
& + \int_0^{L_e} \frac{dN_i}{dz} \frac{2mG\lambda\mu}{1-2\mu} \begin{Bmatrix} -U_c \\ U_r \end{Bmatrix} dz + \int_0^{L_e} N_i \frac{G\lambda^2\mu}{1-\mu} \begin{Bmatrix} W_r \\ W_c \end{Bmatrix} dz \\
& + \int_0^{L_e} N_i \frac{nG\lambda(2-\mu)}{(1-\mu)} \begin{Bmatrix} -dV_c/dz \\ dV_r/dz \end{Bmatrix} dz + \int_0^{L_e} N_i \frac{mG\lambda\mu}{1-\mu} \begin{Bmatrix} -dU_c/dz \\ dU_r/dz \end{Bmatrix} dz \\
& + \int_0^{L_e} N_i \frac{dG}{dz} \frac{m\lambda\mu}{(1-\mu)} \begin{Bmatrix} -U_c \\ U_r \end{Bmatrix} dz + \int_0^{L_e} N_i \frac{dG}{dz} \frac{n\lambda}{1-\mu} \begin{Bmatrix} -V_c \\ V_r \end{Bmatrix} dz \\
& + \int_0^{L_e} N_i \frac{\mu}{(1-\mu)} \begin{Bmatrix} dP_r/dz \\ dP_c/dz \end{Bmatrix} dz
\end{aligned} \tag{50}
$$

$$
\begin{aligned}
N_i \begin{Bmatrix} T_{xyr} \\ T_{xyc} \end{Bmatrix}_0^{L_e} = {} & \int_0^{L_e} \frac{dN_i}{dz} nG\lambda \begin{Bmatrix} -U_c \\ U_r \end{Bmatrix} dz + \int_0^{L_e} \frac{dN_i}{dz} mG\lambda \begin{Bmatrix} -V_c \\ V_r \end{Bmatrix} dz \\
& + \int_0^{L_e} N_i nG\lambda \begin{Bmatrix} -dU_c/dz \\ dU_r/dz \end{Bmatrix} dz + \int_0^{L_e} N_i mG\lambda \begin{Bmatrix} -dV_c/dz \\ dV_r/dz \end{Bmatrix} dz \\
& + \int_0^{L_e} N_i \frac{dG}{dz} n\lambda \begin{Bmatrix} -U_c \\ U_r \end{Bmatrix} dz + \int_0^{L_e} N_i \frac{dG}{dz} m\lambda \begin{Bmatrix} -V_c \\ V_r \end{Bmatrix} dz
\end{aligned} \tag{51}
$$

Introducing equation (38) into equations (35)–(37) and (49)–(51), these can be expressed in matrix form as

$$\{\mathbf{T}\} = \left[\int_0^{L_e} \mathbf{H}_1^{\mathrm{T}} \mathbf{D}_{s1} \mathbf{B}_1 \, \mathrm{d}z + \int_0^{L_e} \mathbf{H}_1^{\mathrm{T}} \mathbf{D}_{s2} \mathbf{B}_2 \, \mathrm{d}z + \int_0^{L_e} \mathbf{H}_2^{\mathrm{T}} \mathbf{D}_{s3} \mathbf{B}_1 \, \mathrm{d}z + \int_0^{L_e} \mathbf{H}_2^{\mathrm{T}} \mathbf{D}_{s4} \mathbf{B}_2 \, \mathrm{d}z \right] \{\mathbf{q}_e\}$$
$$= [\mathbf{H}] \{\mathbf{q}_e\} \tag{52}$$

$$\{\mathbf{T}\}^{\mathrm{T}} = \{-(S_{xr})_1, -(S_{xc})_1, -(S_{yr})_1, -(S_{yc})_1, -(S_{zr})_1, -(S_{zc})_1,$$
$$-(T_{xyr})_1, -(T_{xyc})_1, -(T_{yzr})_1, -(T_{yzc})_1, -(T_{xzr})_1, -(T_{xzc})_1,$$
$$(S_{xr})_{N_p}, (S_{xc})_{N_p}, (S_{yr})_{N_p}, (S_{yc})_{N_p}, (S_{zr})_{N_p}, (S_{zc})_{N_p},$$
$$(T_{xyr})_{N_p}, (T_{xyc})_{N_p}, (T_{yzr})_{N_p}, (T_{yzc})_{N_p}, (T_{xzr})_{N_p}, (T_{xzc})_{N_p}\} \tag{53}$$

$$\mathbf{H}_1 = [H_{11}, H_{12}, H_{13}, \ldots, H_{1n_e}], \quad H_{1i} = H_i \mathbf{I} \tag{54}$$

$$\mathbf{H}_2 = [H_{21}, H_{22}, H_{23}, \ldots, H_{2n_e}], \quad H_{2i} = \frac{\mathrm{d}N_i}{\mathrm{d}z} \mathbf{I} \tag{55}$$

in which $\mathbf{I}$ is a 12×12 identity matrix, and D_{si} ($i = 1, 2, 3, 4$) is a 12×8 matrix (Appendix I).

Following the same procedure, the finite element formulation for the higher-order wave components (i.e. non-linear components) can also be derived. Combining these solutions, the complete solution for wave-induced soil response can then be obtained.

4. RESULTS AND DISSCUSSION

4.1. Effect of element mesh

To examine the influence of element mesh on the accuracy of the present model, three sets of different elements and nodes are chosen as a comparative example. The comparison between the present model and an exact solution[31] is tabulated in Table I. It can be observed from Table I that the first-order results reduced from the present model overall agrees well with the exact solution,[31] even for the coarse mesh. In the following numerical calculation, a three-noded element is used and the number of elements and nodes are chosen as 25 and 51, respectively.

4.2. Verification of the present model

To verify the present numerical model, the reduced results for seabed response due to linear short-crested waves are compared with the previous analytical solution.[31] As shown in Figure 3, the present model (solid lines) agrees well with the analytical solution (dashed lines) for an unsaturated seabed.

Experimental verification using the wave and soil conditions of Nabae sand reported by Maeno[48] is depicted in Figure 4. The results of the empirical formula[48] are also included in the figure (denoted by dashed line). The experimental data are connected in a solid line with circles. The results from the empirical formula might be close to experimental data point at $z/L = -0{\cdot}34$, but it does not predict well near the seabed surface where seabed instability is more likely to occur.[37] On the other hand, the present solution overall agrees with the experimental data throughout the entire soil matrix (Figure 4).

Table I. Test of accuracy of the numerical model[a]

z (m)	Exact solution[b]		Case 1		Case 2		Case 3	
	$\lvert p\rvert/p_0$	$\lvert\sigma'_z\rvert/p_0$	$\lvert p\rvert/p_0$	$\lvert\sigma'_z\rvert/p_0$	$\lvert p\rvert/p_0$	$\lvert\sigma'_z\rvert/p_0$	$\lvert p\rvert/p_0$	$\lvert\sigma'_z\rvert/p_0$
0·0	1·0000	0·0000	1·0000	0·0000	1·0000	0·0000	1·0000	0·0000
− 1·0	0·8675	0·1716	0·8678	0·1718	0·8677	0·1717	0·8676	0·1717
− 2·0	0·7514	0·3153	0·7519	0·3153	0·7513	0·3152	0·7515	0·3151
− 3·0	0·6494	0·4339	0·6499	0·4338	0·6496	0·4335	0·6495	0·4335
− 4·0	0·5596	0·5305	0·5602	0·5302	0·5598	0·5298	0·5597	0·5297
− 5·0	0·4808	0·6077	0·4813	0·6072	0·4810	0·6068	0·4809	0·6066
− 6·0	0·4115	0·6680	0·4120	0·6673	0·4117	0·6668	0·4116	0·6667
− 7·0	0·3509	0·7138	0·3513	0·7129	0·3511	0·7123	0·3511	0·7121
− 8·0	0·2981	0·7469	0·2985	0·7458	0·2984	0·7453	0·2984	0·7451
− 9·0	0·2525	0·7694	0·2529	0·7681	0·2529	0·7675	0·2529	0·7673
− 10·0	0·2136	0·7829	0·2141	0·7813	0·2142	0·7807	0·2143	0·7805
− 11·0	0·1812	0·7888	0·1819	0·7870	0·1821	0·7864	0·1822	0·7862
− 12·0	0·1552	0·7885	0·1563	0·7864	0·1566	0·7859	0·1567	0·7857
− 13·0	0·1357	·07831	0·1372	0·7808	0·1376	0·7803	0·1377	0·7802
− 14·0	0·1227	0·7736	0·1246	0·7711	0·1251	0·7707	0·1252	0·7706
− 15·0	0·1156	0·7610	0·1181	0·7582	0·1186	0·7579	0·1187	0·7578
− 16·0	0·1136	0·7459	0·1167	0·7429	0·1171	0·7427	0·1172	0·7426
− 17·0	0·1156	0·7290	0·1189	0·7258	0·1193	0·7257	0·1194	0·7256
− 18·0	0·1198	0·7108	0·1235	0·7075	0·1237	0·7074	0·1238	0·7073
− 19·0	0·1253	0·6917	0·1292	0·6882	0·1294	0·6882	0·1294	0·6882
− 20·0	0·1311	0·6721	0·1353	0·6685	0·1353	0·6685	0·1353	0·6686
− 21·0	0·1367	0·6523	0·1409	0·6485	0·1409	0·6486	0·1409	0·6486
− 22·0	0·1414	0·6323	0·1457	0·6284	0·1457	0·6286	0·1456	0·6286
− 23·0	0·1450	0·6123	0·1495	0·6084	0·1493	0·6086	0·1493	0·6086
− 24·0	0·1473	0·5924	0·1518	0·5884	0·1516	0·5886	0·1516	0·5887
− 25·0	0·1481	0·5725	0·1527	0·5684	0·1524	0·5686	0·1524	0·5687

[a]Input data: wave period $T = 12{\cdot}0$ s, water depth $d = 50{\cdot}0$ m, wavelength $L = 113{\cdot}27$ m, seabed thickness $h = 25{\cdot}0$ m, Poisson's ratio $\mu = \frac{1}{3}$, porosity $n' = 0{\cdot}3$, shear modulus $G_0 = 10^7$ N/m^2, permeability $k_x = k_y = k_{z0} = 10^{-2}$ m/s, degree of saturation $S_r = 0{\cdot}975$, and wave obliquity $\theta = 45^\circ$

[b]Exact solution is from Reference 31; Case 1 is for two-noded element with 25 elements and 26 nodes; Case 2 is for two-noded element with 50 elements and 51 nodes; Case 3 is for three-noded element with 25 elements and 51 nodes

To further examine the effects of non-linear waves, variable permeability and shear modulus on the wave-induced seabed response, three different seabed materials, gravel, coarse sand and fine sand, are chosen. Although the soil characteristics vary for the same material under different deposition, we only choose the typical values for these materials as examples here. Their soil properties are listed as follows.

(a) Gravel: $G_0 = 5{\cdot}0 \times 10^7$ N/m^2, $K_{z0} = 10^{-1}$ m/s, $\mu = \frac{1}{3}$, $n' = 0{\cdot}3$.
(b) Coarse sand: $G_0 = 10^7$ N/m^2, $K_{z0} = 10^{-2}$ m/s, $\mu = \frac{1}{3}$, $n' = 0{\cdot}3$.
(c) Fine sand: $G_0 = 10^7$ N/m^2, $K_{z0} = 10^{-4}$ m/s, $\mu = \frac{1}{3}$, $n' = 0{\cdot}3$.

4.3. Effects of non-linear wave components

The first aim of this paper concerns with how the non-linear wave components affect the wave-induced soil response. The influence of wave non-linearity on the wave kinematics and

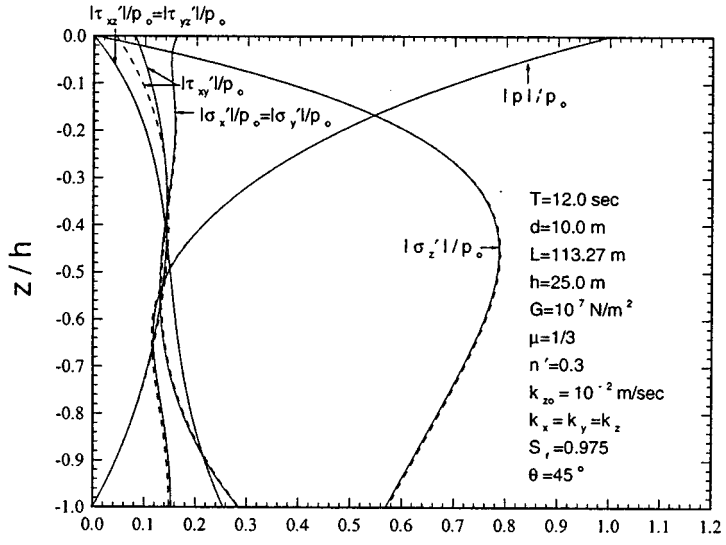

Figure 3. Comparison of the first-order results of the present theory and analytical solution[31] for a partial saturated coarse sand (3-D short-crested wave)

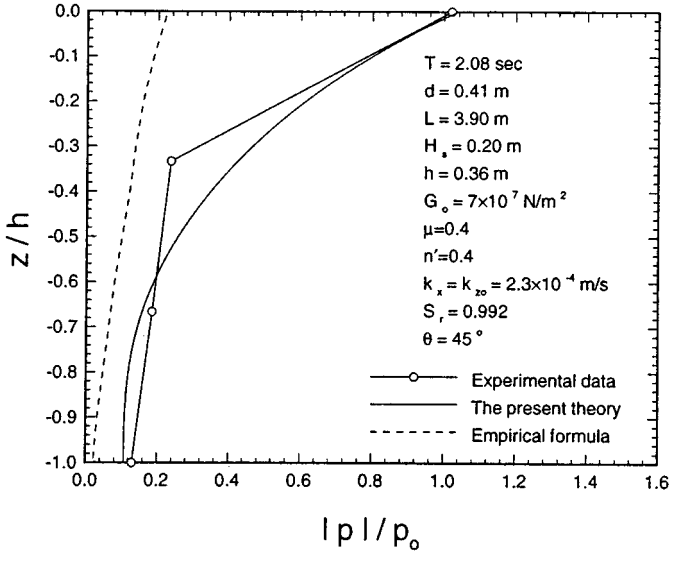

Figure 4. Comparison of the present theory and experimental data[48] (2-D progressive wave)

dynamics have been well documented in the literature.[38,40] However, the influences of non-linear waves on the seabed response have not been examined until now.

As Hsu *et al.*[30] pointed out, the wave-induced pore pressure is independent of the wave obliquity θ, based on the linear wave theory. The vertical distributions of wave induced pore pressure $|p|/p_0$ versus z/h for various wave obliquity θ are tabulated in Table II. The table shows that the magnitude of the wave-induced pore pressure is affected slightly by the wave obliquity θ. These results contrast with the conclusion based on the linear wave theory.[30–36]

Table II. Wave-induced pore pressure $|p|/p_0$ versus z/h for various wave ibliquity θ[a]

z/h	linear	0°	15°	30°	45°	60°	75°	90°
0·0	1·00000	1·55765	1·55765	1·55765	1·55765	1·55765	1·55765	1·55765
− 0·1	0·94688	1·41037	1·41008	1·40962	1·40928	1·40905	1·40891	1·40887
− 0·2	0·88944	1·28865	1·28806	1·28806	1·28653	1·28612	1·28588	1·28580
− 0·3	0·84659	1·11905	1·18957	1·18827	1·18739	1·18684	1·18653	1·18643
− 0·4	0·81212	1·11371	1·11255	1·11090	1·10983	1·10918	1·10882	1·10870
− 0·5	0·78570	1·05622	1·05484	1·05290	1·05167	1·10595	1·05056	1·05043
− 0·6	0·76659	1·01555	1·01399	1·01184	1·01050	1·00973	1·00932	1·00918
− 0·7	0·75378	0·98898	0·98729	0·98498	0·98357	0·98277	0·98234	0·98221
− 0·8	0·74601	0·97347	0·97171	0·96931	0·96786	0·96704	0·96661	0·96647
− 0·9	0·74206	0·96600	0·96420	0·96176	0·96029	0·95947	0·95904	0·95890
− 1·0	0·74088	0·96394	0·96212	0·96967	0·95820	0·95737	0·95694	0·95680

[a]Input data is the same as in Figure 5 and $H_s/L = 0{\cdot}08$

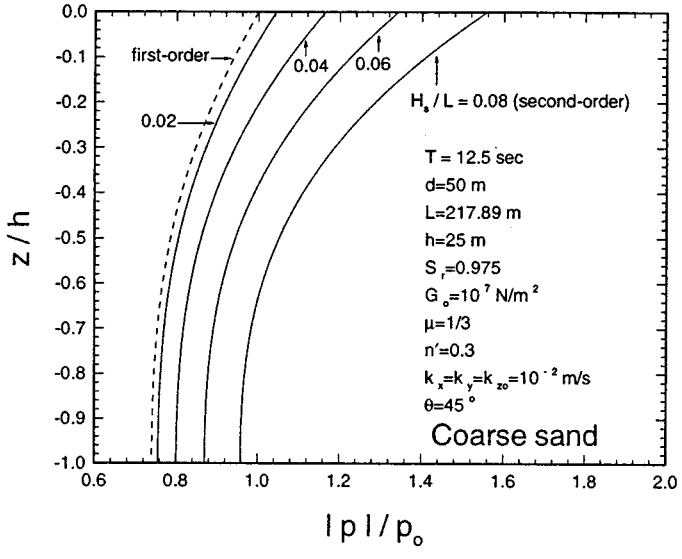

Figure 5. Vertical distribution of the maximum $|p|/p_0$ versus z/h for various wave steepnesses H_s/L

The vertical distribution of the maximum pore pressure amplitude $|p|/p_0$ versus the relative soil depth z/h for various wave steepnesses H_s/L is presented in Figure 5. The soil permeability and shear modulus are considered as uniform here. The wave-induced pore pressure within the porous seabed increases as the wave steepness H_s/L increases. The effect of the second-order component increases as the wave steepness increases (Figure 5). However, this influence decreases as the relative soil depth z/h increases (Figure 6). For example, the relative difference of pore pressure $(|p_2| - |p_1|)/p_0$ decreases from 0·56 at the seabed surface ($z = 0$) to 0·22 at the rigid bottom ($z = -h$) for $H_s/L = 0{\cdot}08$. This implies that the effects of non-linear wave components on the seabed response become significant near the seabed surface.

Figure 7 illustrates the relationship of the maximum amplitude of pore pressure $|p|/p_0$ versus relative soil depths z/h for various relative water depths, d/L. The figure clearly shows that the

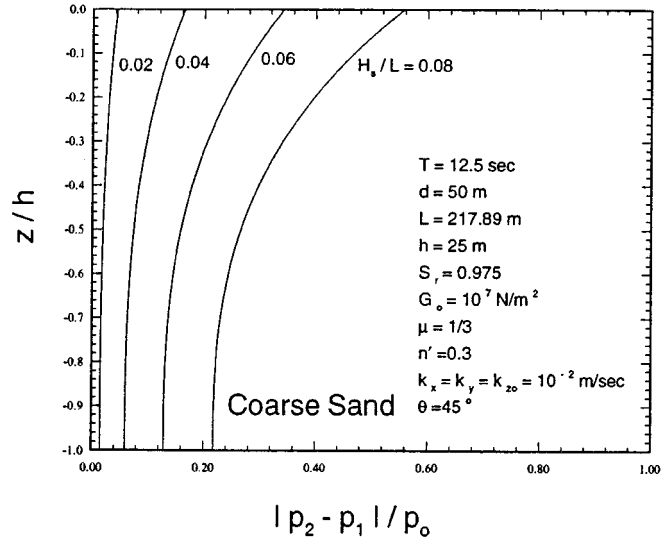

Figure 6. Vertical distribution of the relative difference $(|p_2| - |p_1|)/p_0$ versus z/h for various wave steepnesses H_s/L

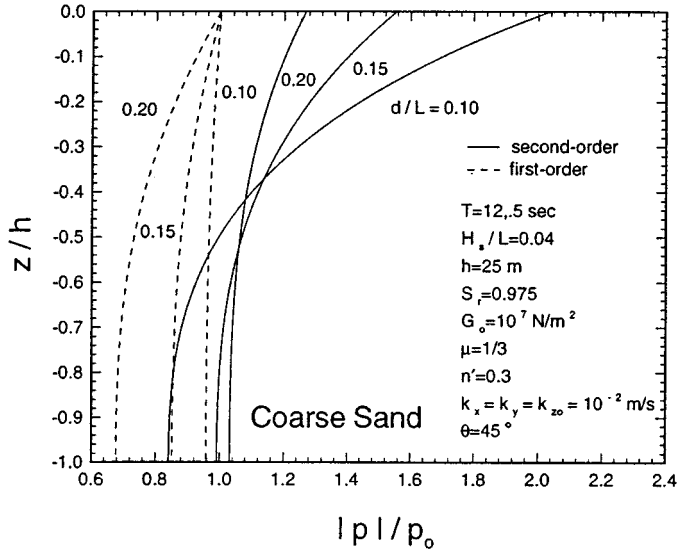

Figure 7. Vertical distribution of the maximum $|p|/p_0$ versus z/h for various relative water depths d/L

wave-induced pore pressure increases as d/L decreases. Furthermore, the relative difference of seabed response due to non-linear wave and linear wave increases as d/L decreases (Figure 8). This implies that the wave-induced seabed reponse is affected more significantly by the non-linear wave components in shallow water than in deep water.

The relationship of the maximum amplitude of pore pressure $|p|/p_0$ versus z/h for different soil types is depicted in Figure 9. The figure shows that the wave-induced pore pressure $|p|/p_0$

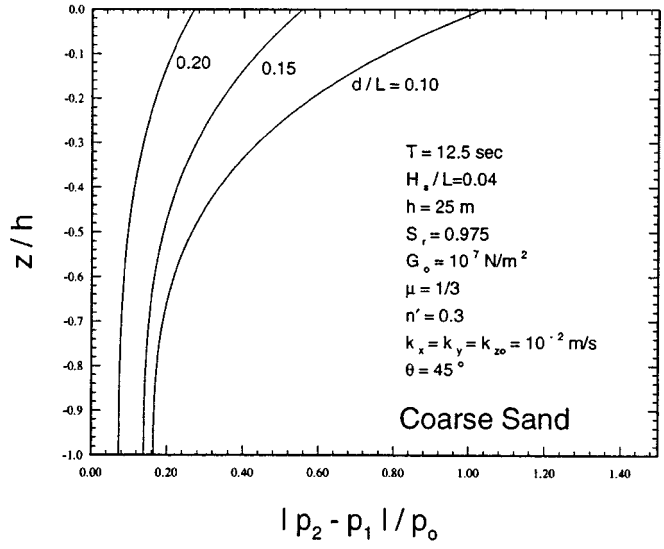

Figure 8. Vertical distribution of the relative difference $(|p_2| - |p_1|)/p_0$ versus z/h for various relative water depths, d/L

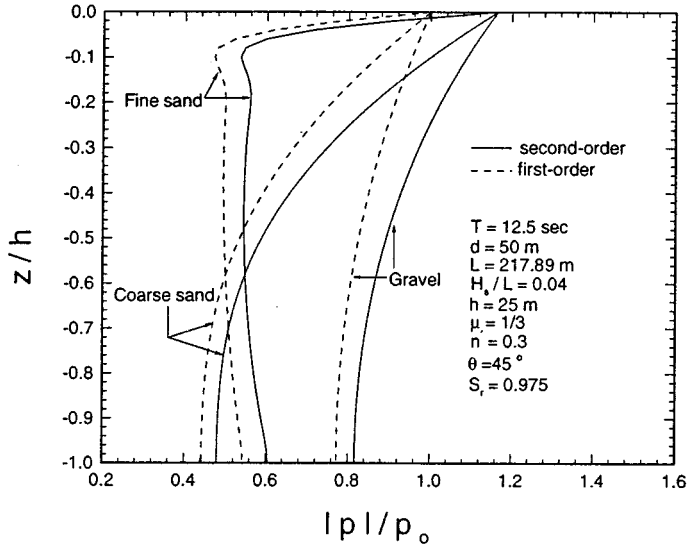

Figure 9. Vertical distribution of the maximum $|p|/p_0$ versus z/h for different soil types

gradually decreases as the soil depth z/h increases for coarse sand and gravelled seabed. However, for the fine sand, the maximum of $|p|/p_0$ decreases rapidly near the seabed surface, and then increases slightly as z/h increases. Figure 9 also shows that the wave-induced pore pressure in gravelled seabeds is larger than in coarse and fine sandy seabeds. Similar trends can also be observed in Figure 10 for the relative difference of pore pressure $(|p_2| - |p_1|)/p_0$.

Air is commonly found within submarine sediments. As the field data[49] show, the degree of saturation (S_r) of marine sediments varies from 0·9 to 1·0 (full saturation). It has been submitted

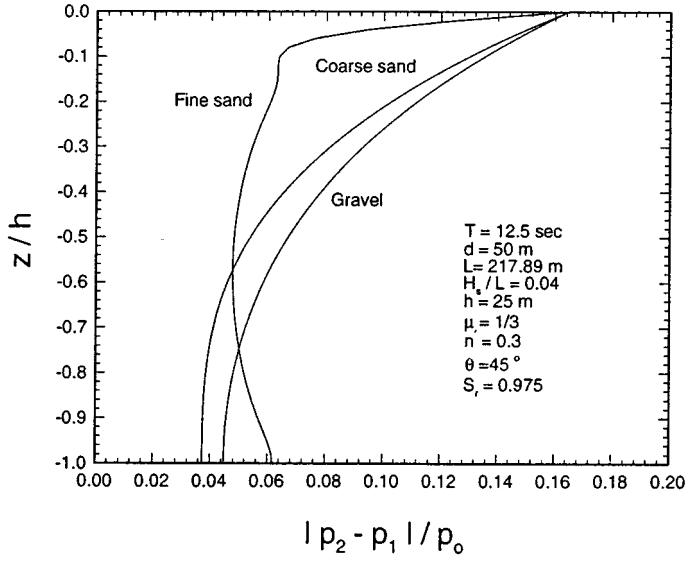

Figure 10. Vertical distribution of the relative difference $(|p_2| - |p_1|)/p_0$ versus z/h for different soil types

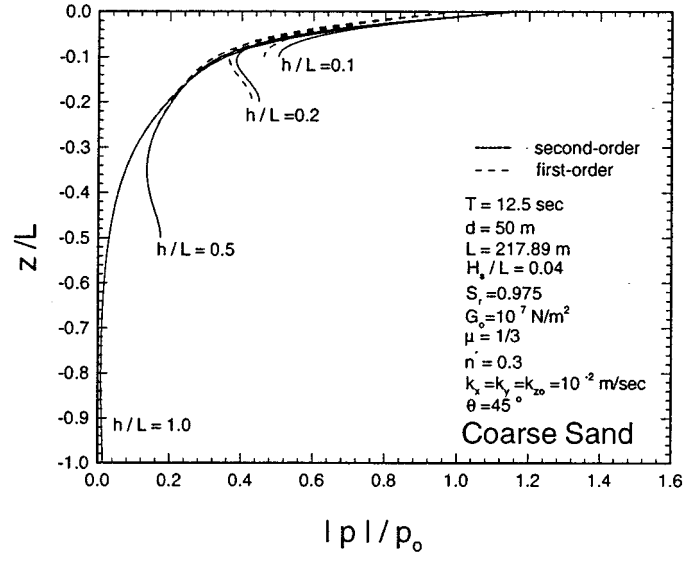

Figure 11. Vertical distribution of the maximum $|p|/p_0$ versus z/h for various degrees of saturation S_r

that the degree of saturation affects the linear wave-induced seabed response significantly.[30] The maximum pore pressure amplitude $|p|/p_0$ decreases as the degree of saturation decreases (Figure 11). Furthermore, similar trends can be found for the relative differences of pore pressure $(|p_2| - |p_1|)/p_0$ (Figure 12). It is important to point out that the wave-induced seabed response is very sensitive to the degree of saturation. For example, the pore pressure for $S_r = 0{\cdot}99$ is about 80 per cent of that for full saturation ($S_r = 1{\cdot}0$) at the rigid bottom ($z = -h$). This implies

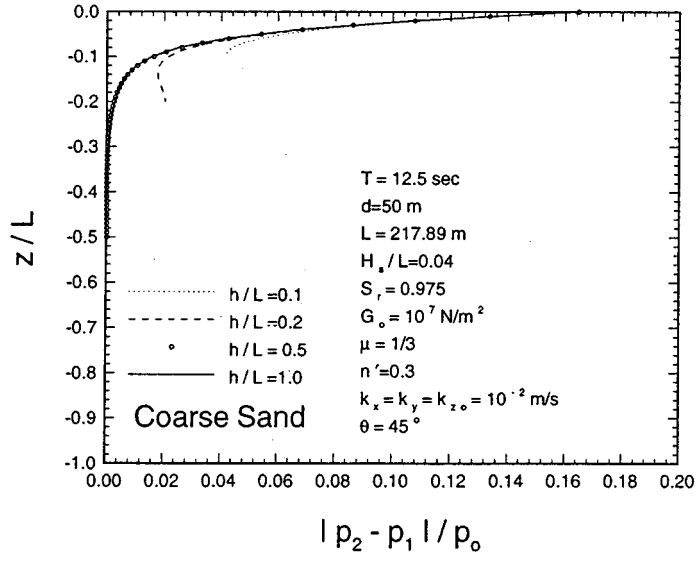

Figure 12. Vertical distribution of the relative difference $(|p_2| - |p_1|)/p_0$ versus z/h for various degrees of saturation S_r

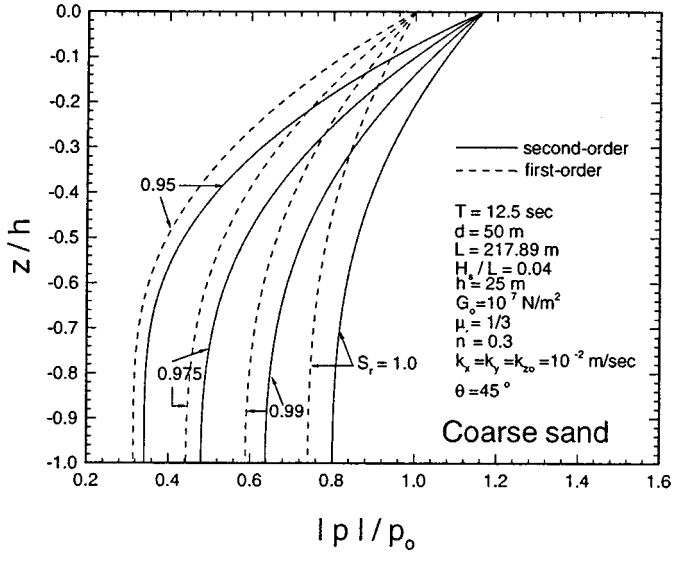

Figure 13. Vertical distribution of the maximum $|p|/p_0$ versus z/L for various relative seabed thicknesses h/L

that the measurements of the degree of saturation in laboratory experiments and field measurements are important. A minor error in estimating the degree of saturation may cause substantial error in estimating wave-induced seabed response.

It has been agreed that the seabed thickness plays an important role in estimating the wave-induced seabed response.[31,35] However, the non-linear wave components only affect the wave-induced pore pressure significantly near the seabed surface for various values of seabed thickness (Figures 13 and 14). This implies that the solution of linear wave-induced seabed

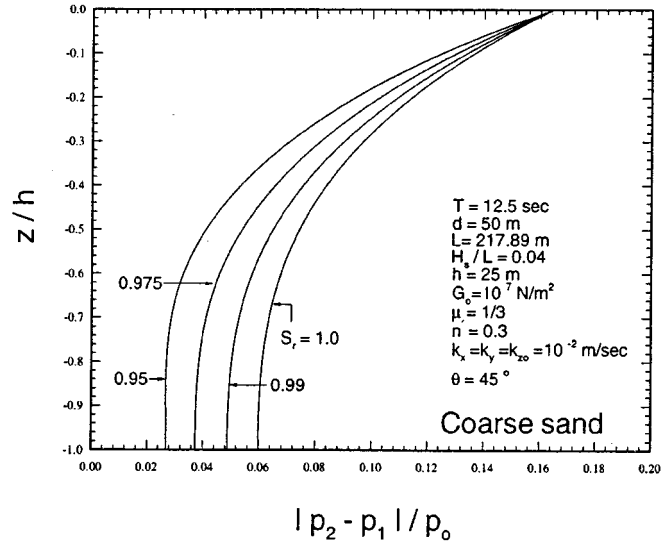

Figure 14. Vertical distribution of the relative difference $(|p_2| - |p_1|)/p_0$ versus z/L for various relative seabed thicknesses h/L

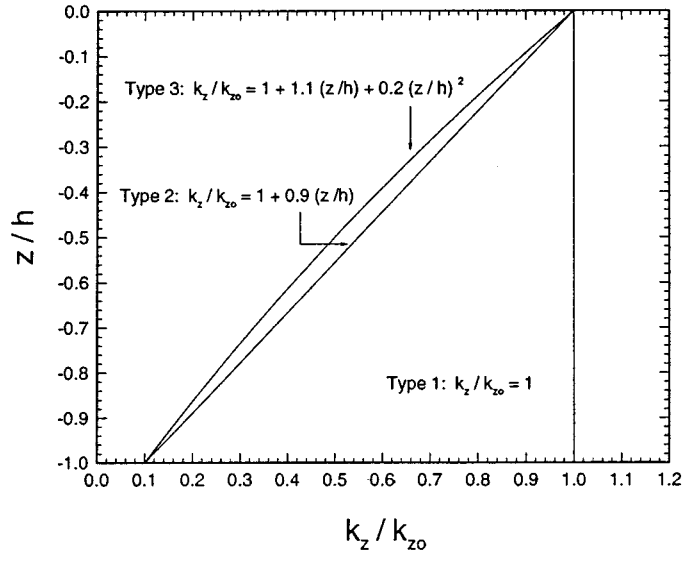

Figure 15. Three different cases of depth function $k_z(z)/k_{z0}$ examined for soil matrix with variable permeability in the present study

response can be used in the deeper region with acceptable errors when the seabed thickness is large. For example, the relative differences of pore pressure $(|p_2| - |p_1|)/p_0$ are less than 2 per cent when the soil depth is deeper than 0·2 times of wavelength for the relative seabed thickness $h/L \geqslant 0{\cdot}2$ (Figure 14).

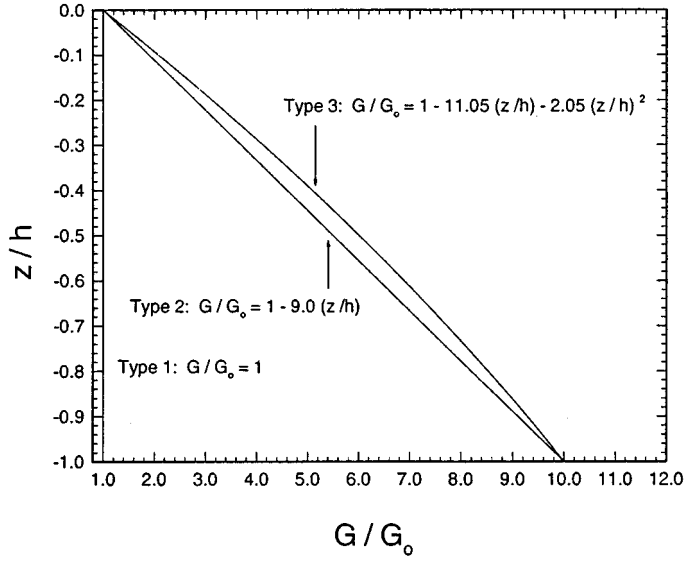

Figure 16. Three different cases of depth function $G(z)|/G_0$ examined for soil matrix with variable shear modulus in the present study

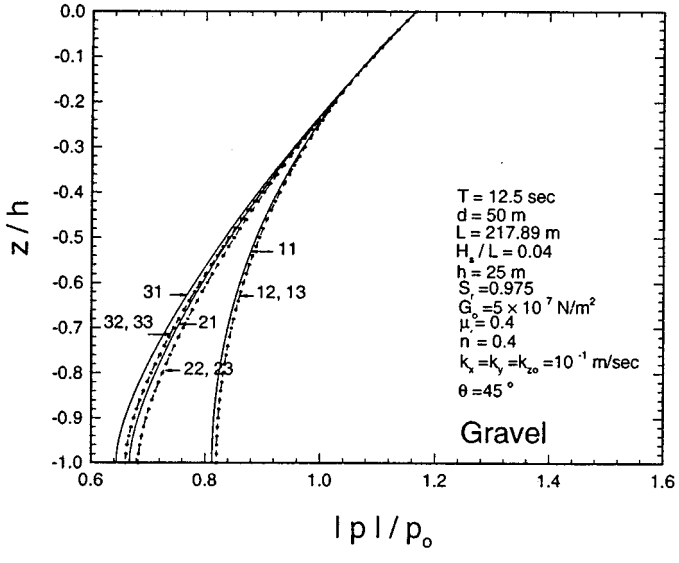

Figure 17. Vertical distribution of the maximum $|p|/p_0$ versus z/h in gravelled seabed

4.4. Effects of variable permeability and shear modulus

The second aim of this study is to examine the effects of variable permeability and shear modulus on the seabed response, respectively. Three different sets of curves are chosen for permeability and shear modulus (Figures 15 and 16). As seen in the figures, Type 1 is a uniform distribution of permeability and shear modulus, which has been considered by conventional

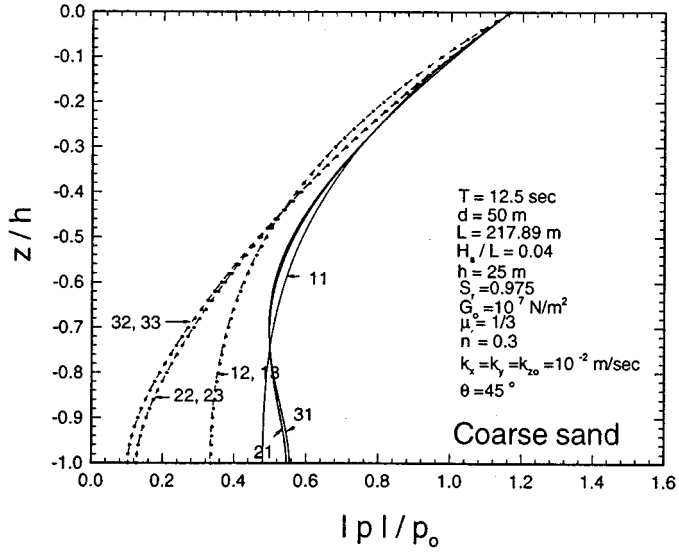

Figure 18. Vertical distribution of the maximum $|p|/p_0$ versus z/h in coarse sand

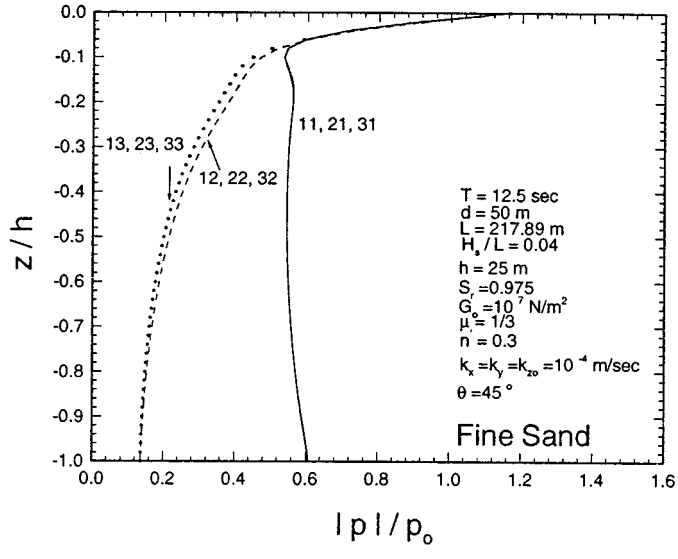

Figure 19. Vertical distribution of the maximum $|p|/p_0$ versus z/h in fine sand

theories. Type 2 is a linear distribution for the ratios k_z/k_{z0} and G/G_0, while Type 3 is a second-order polynomial distribution. It is worth noting that the Type 2 of shear modulus is a kind of *Gibson Soil*, which has been well documented.[43]

The distribution of the maximum amplitude of pore pressure $|p|/p_0$ for different combinations of variable permeability and shear modulus is presented in Figures 17–19 for gravel, coarse and fine sand, respectively. In the figures, the legends '*ij*' denote the Type *i* of variable permeability and Type *j* of variable shear modulus, which are depicted in Figures 15 and 16, respectively.

As Figures 17–19 presented, the normalized pore pressure $|p|/p_0$ is affected significantly by variable permeability for coarse sand and graveled seabed. The calculated results clearly show that the conventional assumption for uniform permeability (i.e. Type 11) does overestimate the pore pressure. However, the wave-induced pore pressure within a seabed of fine sand is unaffected by the variable permeability, because of its low permeability (Figure 19).

As shown in Figures 17–19, the influence of the variable shear modulus on the wave-induced pore pressure is insignificant for the gravelled seabed. However, the effects of shear modulus becomes more significant in fine sand. Similar trends for the influences of variable permeability and shear modulus are observed for other seabed conditions, with different values of the degree of saturation and seabed thickness (not shown in figures). It is surprised that a relative modest increases in shear modulus results in such a dramatic change in pore pressure variation. This unexpected result may raise another interesting subject in the future study.

5. CONCLUSIONS

In this paper, a finite element model has been proposed for analysis of the non-linear waves induced soil response in a porous seabed with variable permeability and shear modulus. Based on the numerical results presented previously, some conclusions may be drawn:

1. Comprehensive verifications of the present theory against the conventional solution[31] and experimental data[48] have been performed.
2. As the numerical results show, the effect of non-linear wave components cannot always be ignored without substantial errors, especially in the region near the seabed surface.
3. It has been submitted that the wave-induced pore pressure is independent of the wave obliquity θ, based on the linear wave theory.[30] However, this conclusion is invalid for the soil response due to non-linear waves, as shown in Table II.
4. The degree of saturation, soil type and seabed thickness also affect the relative differences of the pore pressure due to linear and non-linear waves. For example, the pore pressure which is caused by non-linear waves is almost identical with that due to linear wave, when the relative seabed thickness h/L is greater than 0·2.
5. For a seabed of coarser material, such as gravel and coarse sand, the wave-induced pore pressure is affected significantly by variable permeability. On the other hand, it is affected remarkably by variable shear modulus in a finer seabed.

In this study, only non-linear wave-induced pore pressure has been investigated. The more detailed parametric study for the resulting seabed stability analysis has not been considered here. Based on the present model, it is worthwhile to examine the influence of variable soil characteristics on such practical application in the near future.

ACKNOWLEDGEMENTS

The author wishes to thank the reviewers and Dr. H. Zhang of the University of Western Australia for their helpful comments.

APPENDIX I

List of coefficients matrices $\mathbf{D}_i$ *and* $\mathbf{D}_{si}$

The coefficients matrices $\mathbf{D}_i$ of equation (43) are listed as follows:

$$\mathbf{D}_1 =$$

$$\begin{bmatrix}
\dfrac{m^2\lambda^2 k_x + n^2\lambda^2 k_y}{k_z} & \dfrac{\gamma_w n'\beta\omega}{k_z} & \dfrac{m\lambda\gamma_w\omega}{k_z} & 0 & \dfrac{n\lambda\gamma_w\omega}{k_z} & 0 & 0 & 0 \\
-\dfrac{\gamma_w n'\beta\omega}{k_z} & \dfrac{m^2\lambda^2 k_x + n^2\lambda^2 k_y}{k_z} & 0 & \dfrac{m\lambda\gamma_w\omega}{k_z} & 0 & \dfrac{n\lambda\gamma_w\omega}{k_z} & 0 & 0 \\
0 & -mk & G\left(\lambda^2 + \dfrac{m^2\lambda^2}{1-2\mu}\right) & 0 & \dfrac{nmG\lambda^2}{1-2\mu} & 0 & 0 & 0 \\
m\lambda & 0 & 0 & G\left(\lambda^2 + \dfrac{m^2\lambda^2}{1-2\mu}\right) & 0 & \dfrac{nmG\lambda^2}{1-2\mu} & 0 & 0 \\
0 & -nk & \dfrac{nmG\lambda^2}{1-2\mu} & 0 & G\left(\lambda^2 + \dfrac{n^2\lambda^2}{1-2\mu}\right) & 0 & 0 & 0 \\
nk & 0 & 0 & \dfrac{nmG\lambda^2}{1-2\mu} & 0 & G\left(\lambda^2 + \dfrac{n^2\lambda^2}{1-2\mu}\right) & 0 & 0 \\
0 & 0 & 0 & 0 & 0 & 0 & G\lambda^2 & 0 \\
0 & 0 & 0 & 0 & 0 & 0 & 0 & G\lambda^2
\end{bmatrix} \tag{51}$$

$$\mathbf{D}_2 = \begin{bmatrix}
-k_z\dfrac{\mathrm{d}k_z}{\mathrm{d}z} & 0 & 0 & 0 & 0 & 0 & 0 & \dfrac{\gamma_w\omega}{k_z} \\
0 & -k_z\dfrac{\mathrm{d}k_z}{\mathrm{d}z} & 0 & 0 & 0 & 0 & -\dfrac{\gamma_w\omega}{k_z} & 0 \\
0 & 0 & 0 & 0 & 0 & 0 & 0 & \dfrac{2mG\lambda\mu}{1-2\mu} \\
0 & 0 & 0 & 0 & 0 & 0 & -\dfrac{2mG\lambda\mu}{1-2\mu} & 0 \\
0 & 0 & 0 & 0 & 0 & 0 & 0 & \dfrac{2nG\lambda\mu}{1-2\mu} \\
0 & 0 & 0 & 0 & 0 & 0 & -\dfrac{2nG\lambda\mu}{1-2\mu} & 0 \\
1 & 0 & 0 & Gm\lambda & 0 & Gn\lambda & 0 & 0 \\
0 & 1 & -Gm\lambda & 0 & -Gn\lambda & 0 & 0 & 0
\end{bmatrix} \tag{52}$$

$$\mathbf{D}_3 = \begin{bmatrix}
0 & 0 & 0 & 0 & 0 & 0 & 0 & 0 \\
0 & 0 & 0 & 0 & 0 & 0 & 0 & 0 \\
0 & 0 & 0 & 0 & 0 & 0 & 0 & -Gm\lambda \\
0 & 0 & 0 & 0 & 0 & 0 & Gm\lambda & 0 \\
0 & 0 & 0 & 0 & 0 & 0 & 0 & -Gn\lambda \\
0 & 0 & 0 & 0 & 0 & 0 & Gn\lambda & 0 \\
0 & 0 & 0 & -\dfrac{2Gm\lambda\mu}{1-2\mu} & 0 & -\dfrac{2Gn\lambda\mu}{1-2\mu} & 0 & 0 \\
0 & 0 & \dfrac{2Gm\lambda\mu}{1-2\mu} & 0 & \dfrac{2Gn\lambda\mu}{1-2\mu} & 0 & 0 & 0
\end{bmatrix} \tag{53}$$

$$\mathbf{D}_4 = \begin{bmatrix} 1 & 0 & 0 & 0 & 0 & 0 & 0 & 0 \\ 0 & 1 & 0 & 0 & 0 & 0 & 0 & 0 \\ 0 & 0 & G & 0 & 0 & 0 & 0 & 0 \\ 0 & 0 & 0 & G & 0 & 0 & 0 & 0 \\ 0 & 0 & 0 & 0 & G & 0 & 0 & 0 \\ 0 & 0 & 0 & 0 & 0 & G & 0 & 0 \\ 0 & 0 & 0 & 0 & 0 & 0 & \dfrac{2G(1-\mu)}{1-2\mu} & 0 \\ 0 & 0 & 0 & 0 & 0 & 0 & 0 & \dfrac{2G(1-\mu)}{1-2\mu} \end{bmatrix} \tag{54}$$

The coefficients matrices $\mathbf{D}_{si}$ of equation (52) are listed as follows:

$\mathbf{D}_{s1} =$

$$\begin{bmatrix} 0 & 0 & 0 & -\dfrac{\mathrm{d}G}{\mathrm{d}z}\dfrac{m\lambda}{1-\mu} & 0 & -\dfrac{\mathrm{d}G}{\mathrm{d}z}\dfrac{n\lambda\mu}{1-\mu} & \dfrac{G\lambda^2\mu}{1-\mu} & 0 \\ 0 & 0 & \dfrac{\mathrm{d}G}{\mathrm{d}z}\dfrac{m\lambda}{1-\mu} & 0 & \dfrac{\mathrm{d}G}{\mathrm{d}z}\dfrac{n\lambda\mu}{1-\mu} & 0 & 0 & \dfrac{G\lambda^2\mu}{1-\mu} \\ 0 & 0 & 0 & -\dfrac{\mathrm{d}G}{\mathrm{d}z}\dfrac{mk\mu}{1-\mu} & 0 & -\dfrac{\mathrm{d}G}{\mathrm{d}z}\dfrac{n\lambda\mu}{1-\mu} & \dfrac{G\lambda^2\mu}{1-\mu} & 0 \\ 0 & 0 & \dfrac{\mathrm{d}G}{\mathrm{d}z}\dfrac{m\lambda\mu}{1-\mu} & 0 & \dfrac{\mathrm{d}G}{\mathrm{d}z}\dfrac{n\lambda}{1-\mu} & 0 & 0 & \dfrac{G\lambda^2\mu}{1-\mu} \\ 0 & 0 & 0 & 0 & 0 & 0 & G\lambda^2 & 0 \\ 0 & 0 & 0 & 0 & 0 & 0 & 0 & G\lambda^2 \\ 0 & 0 & 0 & -\dfrac{\mathrm{d}G}{\mathrm{d}z}n\lambda & 0 & -\dfrac{\mathrm{d}G}{\mathrm{d}z}m\lambda & 0 & 0 \\ 0 & 0 & \dfrac{\mathrm{d}G}{\mathrm{d}z}n\lambda & 0 & \dfrac{\mathrm{d}G}{\mathrm{d}z}m\lambda & 0 & 0 & 0 \\ 0 & -n\lambda & \dfrac{mnG\lambda^2}{1-2\mu} & 0 & G\left(\lambda^2+\dfrac{n^2\lambda^2}{1-2\mu}\right) & 0 & 0 & 0 \\ n\lambda & 0 & 0 & \dfrac{mnG\lambda^2}{1-2\mu} & 0 & G\left(\lambda^2+\dfrac{n^2\lambda^2}{1-2\mu}\right) & 0 & 0 \\ 0 & -m\lambda\, G\left(\lambda^2+\dfrac{n^2\lambda^2}{1-2\mu}\right) & 0 & \dfrac{mnG\lambda^2}{1-2\mu} & 0 & 0 & 0 & 0 \\ m\lambda & 0 & 0 & G\left(\lambda^2+\dfrac{m^2\lambda^2}{1-2\mu}\right) & 0 & \dfrac{mnG\lambda^2}{1-2\mu} & 0 & 0 \end{bmatrix} \tag{55}$$

$$\mathbf{D}_{s2} =$$

$$\begin{bmatrix}
\frac{\mu}{1-\mu} & 0 & 0 & -\frac{mG\lambda(2-\mu)}{(1-\mu)} & 0 & -\frac{nG\lambda\mu}{1-\mu} & 0 & 0 \\
0 & \frac{\mu}{1-\mu} & \frac{mG\lambda(2-\mu)}{(1-\mu)} & 0 & -\frac{nG\lambda\mu}{1-\mu} & 0 & 0 & 0 \\
\frac{\mu}{1-\mu} & 0 & 0 & -\frac{mG\lambda\mu}{1-\mu} & 0 & -\frac{nG\lambda(2-\mu)}{(1-\mu)} & 0 & 0 \\
0 & \frac{\mu}{1-\mu} & \frac{mG\lambda\mu}{1-\mu} & 0 & -\frac{nG\lambda(2-\mu)}{(1-\mu)} & 0 & 0 & 0 \\
1 & 0 & 0 & Gm\lambda & 0 & Gn\lambda & 0 & 0 \\
0 & 1 & -Gm\lambda & 0 & -Gn\lambda & 0 & 0 & 0 \\
0 & 0 & 0 & -Gn\lambda & 0 & -Gm\lambda & 0 & 0 \\
0 & 0 & Gn\lambda & 0 & Gm\lambda & 0 & 0 & 0 \\
0 & 0 & 0 & 0 & 0 & 0 & 0 & \frac{2nG\lambda\mu}{1-2\mu} \\
0 & 0 & 0 & 0 & 0 & 0 & -\frac{2nG\lambda\mu}{1-2\mu} & 0 \\
0 & 0 & 0 & 0 & 0 & 0 & 0 & \frac{2mG\lambda\mu}{1-2\mu} \\
0 & 0 & 0 & 0 & 0 & 0 & -\frac{2mG\lambda\mu}{1-2\mu} & 0
\end{bmatrix} \tag{56}$$

$$\mathbf{D}_{s3} =$$

$$\begin{bmatrix}
0 & 0 & 0 & -\frac{2Gm\lambda(1-\mu)}{1-2\mu} & 0 & -\frac{2nG\lambda\mu}{1-2\mu} & 0 & 0 \\
0 & 0 & \frac{2Gm\lambda(1-\mu)}{1-2\mu} & 0 & \frac{2nG\lambda\mu}{1-2\mu} & 0 & 0 & 0 \\
0 & 0 & 0 & -\frac{2Gm\lambda\mu}{1-2\mu} & 0 & -\frac{2nG\lambda(1-\mu)}{1-2\mu} & 0 & 0 \\
0 & 0 & \frac{2Gm\lambda\mu}{1-2\mu} & 0 & \frac{2nG\lambda(1-\mu)}{1-2\mu} & 0 & 0 & 0 \\
0 & 0 & 0 & -\frac{2mG\lambda\mu}{1-2\mu} & 0 & -\frac{2nG\lambda\mu}{1-2\mu} & 0 & 0 \\
0 & 0 & \frac{2mG\lambda\mu}{1-2\mu} & 0 & \frac{2nG\lambda\mu}{1-2\mu} & 0 & 0 & 0 \\
0 & 0 & 0 & -nG\lambda & 0 & -mG\lambda & 0 & 0 \\
0 & 0 & nG\lambda & 0 & mG\lambda & 0 & 0 & 0 \\
0 & 0 & 0 & 0 & 0 & 0 & 0 & -nG\lambda \\
0 & 0 & 0 & 0 & 0 & 0 & nG\lambda & 0 \\
0 & 0 & 0 & 0 & 0 & 0 & 0 & -mG\lambda \\
0 & 0 & 0 & 0 & 0 & 0 & mG\lambda & 0
\end{bmatrix} \tag{57}$$

$$\mathbf{D}_{s4} = \begin{bmatrix} 0 & 0 & 0 & 0 & 0 & 0 & \dfrac{2G\mu}{1-2\mu} & 0 \\ 0 & 0 & 0 & 0 & 0 & 0 & 0 & \dfrac{2G\mu}{1-2\mu} \\ 0 & 0 & 0 & 0 & 0 & 0 & \dfrac{2G\mu}{1-2\mu} & 0 \\ 0 & 0 & 0 & 0 & 0 & 0 & 0 & \dfrac{2G\mu}{1-2\mu} \\ 0 & 0 & 0 & 0 & 0 & 0 & \dfrac{2G(1-\mu)}{1-2\mu} & 0 \\ 0 & 0 & 0 & 0 & 0 & 0 & 0 & \dfrac{2G(1-\mu)}{1-2\mu} \\ 0 & 0 & 0 & 0 & 0 & 0 & 0 & 0 \\ 0 & 0 & 0 & 0 & G & 0 & 0 & 0 \\ 0 & 0 & 0 & 0 & 0 & G & 0 & 0 \\ 0 & 0 & G & 0 & 0 & 0 & 0 & 0 \\ 0 & 0 & 0 & 0 & G & 0 & 0 & 0 \end{bmatrix} \tag{58}$$

APPENDIX II

Notation

d	water depth
E	Young modulus
f	general function of soil response
G	shear modulus
h	seabed thickness
H_s	wave height
i	complex number $(=\sqrt{-1})$
$\mathbf{I}$	identity matrix
k_x, k_y, k_z	hydraulic permeability in x-, y- and z-directions
K'	apparent bulk modulus of the pore water
K_w	true bulk modulus of elasticity of water
L	wavelength
L_e	length of the element
L_x, L_y	wavelength and crest length of the short-crested waves, as seen in Figure 1
m, n	obliquity parameters
n'	porosity
N_i	shape function of the ith node
N_p	total number of nodal points
p	pore pressure
P_b	wave pressure at seabed surface
P_{w0}	absolute pore-water pressure
P_0	amplitude of linear wave pressure at seabed surface
S_r	degree of saturation

t	time
T	wave period
u, v, w	soil displacements in x-, y-, and z-directions
x, y, z	Cartesian co-ordinates

Greek letters

β	compressibility of pore fluid
γ_w	unit weight of water
ε	volume strain of soil (see equation (2))
θ	wave obliquity
λ	wave number
λ_x, λ_y	components of wave number k in x- and y-directions
μ	Poisson's ratio
$\sigma'_x, \sigma'_y, \sigma'_z$	effective normal stresses
$\tau'_{xy}, \tau'_{xz}, \tau'_{yz}$	effective shear stresses

Subscripts

a	component of reflected waves
b	component of incident waves
c	imaginary part of complex variable
i	ith node
r	real part of complex variable
0	physical properties at the seabed surface, e.g. K_{z0}, G_0

REFERENCES

1. M. S. Rahman, 'Wave-induced instability of seabed: mechanism and conditions', *Mar. Geotechnol.* **10,** 277–299 (1991).
2. H. Nago, S. Maeno, T. Matsumoto and Y. Hachiman, 'Liquefaction and desification of loosely deposited sand bed under water pressure variation', *Proc. 3rd (1993) Int. Offshore and Polar Engineering Conf.* Singapore, 1993, pp. 578–584.
3. K. Zen and H. Yamazaki, 'Field observation and analysis of wave-induced liquefaction in seabed', *Soils Found.*, **31**(4), 161–179 (1991).
4. J. A. Putnam, 'Loss of wave energy due to percolation in a permeable sea bottom', *Trans. Am. Geophys. Union*, **30,** 77–133 (1949).
5. P. L. F. Liu, 'Damping of water waves over porous bed', *J. Hydraul. Div. ASCE*, **3** (HY12), 2263–2271 (1973).
6. J. F. A. Sleath, 'Wave-induced pressure coefficients in beds of sand', *J. Hydraul. Div. ASCE*, **96** (HY2), 367–378 (1970).
7. P. L. F. Liu, 'On gravity waves propagated over a layered permeable bed', *Coastal Eng.*, **1,** 135–148 (1977).
8. H. Moshagen and A. Torum, 'Wave induced pressures in permeable seabeds', *J. Waterways Harbour Coastol Eng. Div. ASCE*, **101** (WW1), 49–58 (1975).
9. M. A. Biot, 'General theory of three-dimensional consolidation', *J. Appl. Phys.* **12,** 155–164 (1941).
10. A. Verruijt, 'Elastic storage of aquifers', in R. J. M. De Wiest (ed.), *Flow Through Porous Media*, Academic Press, New York, Chapter 8, pp. 331–376.
11. T. Yamamoto, 'Wave induced instability in seabeds', *Proc. Coastal Sediments '77, ASCE* 1977, pp. 898–913.
12. T. Yamamoto, H. L. Koning, H. Sellmeiher and E. V. van Hijum, 'On the response of a poro-elastic bed to water waves', *J Fluid Mech.* **87,** 193–206 (1978).
13. T. Yamamoto, 'Wave-induced pore pressure and effective stresses in inhomogeneous seabed foundations', *Ocean Eng.*, **8,** 1–16 (1981).
14. S. Okusa, 'Wave-induced stresses in unsaturated submarine sediments', *Géotechnique*, **35,** 517–532 (1985).
15. O. S. Madsen, 'Wave-induced pore pressures and effective stresses in a porous bed', *Géotechnique*, **28,** 377–393 (1978).
16. D. S. Jeng and B. R. Seymour, 'Wave-induced pore pressure and effective stresses in a porous seabed with variable permeability', *Proc. 15th Int. Conf. on Offshore Mechanics and Arctic Engineering, ASME*, Florence, Italy, 16–20 June 1996, pp. 327–334.
17. D. S. Jeng, 'Wave-induced liquefaction potential in a cross-anisotropic seabed', *J. Chin. Inst. Eng.*, **19**(1), 59–70 (1996).

18. D. S. Jeng, 'Soil response in a cross-anisotropic seabed due to standing waves', *J. Geotech. Eng. ASCE*, in press.
19. K. Zen and H. Yamazaki, 'Mechanism of wave-induced liquefaction and densification in seabed', *Soils Found.*, **30**(4), 90–104 (1990).
20. W. Magda, 'Study on one-dimensional model for wave-induced pore-water pressure', *Proc. 4th Russian Conf. with Foreign Participation*, St. Petersburg, 1993, pp. 179–191.
21. B. Gatmiri, 'A simplified finite element analysis of wave-induced effective stresses and pore pressures in permeable sea beds', *Géotechnique*, **40,** 15–30 (1990).
22. S. D. Thomas, 'A finite element model for the analysis of wave induced stresses, displacements and pore pressures in an unsaturated seabed II: Model verification', *Comput. Geotech.* **17,** 107–132 (1995).
23. W. Raman-Nair and G. C. W. Sabin, 'Wave-induced failure of poroelastic seabed slope: a boundary element study', *Proc. Inst. Civil Eng.* Part 2, **91,** 771–794 (1991).
24. J. D. Fenton, 'Wave forces on vertical walls', *J. Waterway Port Coastal Ocean Eng. ASCE*, **111**(4), 693–718 (1985).
25. C. P. Tsai and D. S. Jeng, 'A Fourier approximation for finite amplitude short-crested waves in deep water', *J. Chin. Inst. Eng.*, **15,** 713–721 (1992).
26. C. P. Tsai, D. S. Jeng and J. R. C. Hsu, 'Computations of the almost highest short-crested waves in deep water', *Appl. Ocean Res.*, **16** (6), 317–326 (1994).
27. A. W. Smith and A. D. Gordon, 'Large breakwater toe failures', *J. Waterway Port Coastal Ocean Eng. ASCE*, **109,** 253–255 (1983).
28. R. Silvester and J. R. C. Hsu, 'Sines revisited', *J. Waterways Port Coastal Ocean Eng. ASCE*, **115** (3), 327–344 (1989).
29. H. Lundgren, H. C. Lindhardt Jacobsen and C. J. Romhild, 'Stability of breakwaters on poor foundations', *Proc. 12th Int. Conf. on Soil Mechanics and Foundation Engineering*, 1989, pp. 451–454.
30. J. R. C. Hsu, D. S. Jeng and C. P. Tsai, 'Short-crested wave induced soil response in a porous seabed of infinite thickness', *Int. j. numer. anal. methods geomech.*, **17,** 553–576 (1993).
31. J. R. C. Hsu and D. S. Jeng, 'Wave-induced soil response in an unsaturated anisotropic seabed of finite thickness', *Int. j. numer. anal. methods geomech.*, **18,** 785–807 (1994).
32. M. S. Rahman, K. El-Zahaby and J. Booker, 'A semi-analytical method for the wave-induced seabed response', *Int. j. numer. Anal. Methods Geomech.*, **18,** 213–236 (1994).
33. J. R. C. Hsu, D. S. Jeng and C. P. Lee, 'Oscillatory soil response and liquefaction in an unsaturated layered seabed', *Int. j. numer. anal. methods geomech.*, **19,** 825–849 (1995).
34. B. R. Seymour, D. S. Jeng and J. R. C. Hsu, 'Transient soil response in a porous seabed with variable permeability', *Ocean Eng.*, **23**(1), 27–46 (1996).
35. D. S. Jeng and J. R. C. Hsu, 'Wave-induced soil response in a nearly saturated seabed of finite thickness', *Géotechnique*, in press.
36. D. S. Jeng and Y. S. Lin, 'Finite element modelling for water waves-soil interaction', *Soil Dyn. Earthquake Eng.*, in press.
37. D. S. Jeng, 'Wave-induced seabed instability in front of a breakwater', *Ocean Eng.*, in press.
38. T. Ohyama, D. S. C. Jeng and J. R. C. Hsu, 'Fourth-order theory for multiple-wave interaction', *Coastal Eng.*, **25,** 43–63 (1995).
39. R. G. Dean, 'Relative validities of water wave theories', *J. Waterways Harbors Coastal Eng. Div. ASCE*, **96** (WW1), 105–119 (1970).
40. N. E. Huang, S. R. Long, C. C. Tung, Y. Yuan and L. F. Bliven, 'A non-Gaussian statistical model for surface elevation of nonlinear random wave fields', *J. Geophys. Res.*, **88**(C12), 7597–7606 (1983).
41. W. R. Bryant, W. Hottman and P. Trabant, 'Permeability of unconsolidated and consolidated marine sediments, Gulf of Mexico', *Mar. Geotechnol.*, **1,** 1–15 (1974).
42. R. H. Bennett, H. Li, D. N. Lambert, K. M. Fischer, D. J. Waler, C. E. Hickox, M. H. Hulbert, T. Yamamoto and M. Badiey, '*In situ* porosity and permeability of selected carbonate sediment: Great Bahaman Bank. Part 1: Measurements', *Mar. Geotechnol.*, **9,** 1–28 (1990).
43. R. E. Gibson, 'Some results concerning displacements and stresses in a non-homogeneous elastic half-space', *Géotechnique*, **17,** 58–67 (1967).
44. M. Badiey, K. Zen, H. Yamazaki and H. Suzuki, 'Field and laboratory measurements of shear modulus profile in seabed', *Report Port Harbour Inst. Japan*, **29**(4), 3–26 (1990).
45. J. R. C. Hsu, Y. Tsuchiya and R. Silvester, 'Third-order approximation to short-crested waves' *J. Fluid Mech.*, **90,** 179–196 (1979).
46. R. J. Sobey, P. Goodwin, R. J. Thieke and R. J. Westberg Jr., 'Application of Stokes, Cnoidal and Fourier wave theories', *J. Waterway, Port, Coastal and Ocean Eng. ASCE*, **113**(6), 565–587 (1987).
47. O. C. Zienkiewicz and R. L. Taylor, *The Finite Element Method*, Fourth Edition, McGraw-Hill, London, 648pp.
48. Y. H. Maeno, 'Effect of energy loss near bed surface on wave-induced pore pressure in sand layer', *Proc. 21st Coastal Engineering Conf. ASCE*, Spain, 1988 pp. 1842–1856.
49. M. I. Esrig, M. I. and R. C. Kirbym, 'Implications of gas content for predicting the stability of submarine slopes', *Mar. Geotechnol.*, **2,** 81–100 (1977).